

**Pressure-induced amorphization of methane hydrate**Niall J. English<sup>1,\*</sup> and John S. Tse<sup>2,†</sup><sup>1</sup>*SEC Strategic Research Cluster and Centre for Synthesis and Chemical Biology, School of Chemical and Bioprocess Engineering, University College Dublin, Belfield, Dublin 4, Ireland*<sup>2</sup>*Department of Physics and Engineering Physics, University of Saskatchewan, Saskatoon, Saskatchewan, Canada S7N 5E2*  
(Received 13 October 2011; published 18 September 2012)

Pressure-induced amorphization of methane hydrate has been investigated by molecular dynamics simulation. In accord with experimental results of Tulk *et al.*, a crystalline  $\rightarrow$  amorphous transition was confirmed at 3.3 GPa where the water lattice collapsed around the encaged methane. Thermal annealing at 5.5 GPa allows the water to adopt a lower energy conformation with a denser structure. In both structures, methane molecules are immobilized and maintain long-range correlation as in the crystal. Consequently, both phases are predicted to revert back to the crystalline form upon decompression. Pressure-induced amorphization is a nonequilibrium process due to a mechanical instability; the interconversion between kinetically stable amorphous phases is a relaxation effect.

DOI: [10.1103/PhysRevB.86.104109](https://doi.org/10.1103/PhysRevB.86.104109)

PACS number(s): 61.43.-j, 61.50.Ks, 63.20.-e

The two-liquid hypothesis of water<sup>1</sup> was based on observing low-temperature pressure amorphization of ice into a high-density form (HDA)<sup>2</sup> and subsequent conversion to a low-density form (LDA) upon heating.<sup>3</sup> It is reckoned that HDA formation occurs via thermodynamic melting.<sup>4</sup> Further, if the HDA  $\rightarrow$  LDA transformation is first order, extrapolation of the phase boundary of the purportedly distinct phases into the liquid region will terminate at a critical point;<sup>1,4</sup> this would support the view that liquid water structure arises from the coexistence of low- and high-density liquid phases. However, this proposition, along with underlying mechanisms of pressure-induced amorphization, has been the subject of much controversy; a different viewpoint on pressure-induced amorphization arises from considering it as violating Born's stability criteria,<sup>5,6</sup> with ice structure collapse into a metastable frustrated disordered structure.<sup>7</sup> Apart from theoretical evidence, the latter explanation has gained support from recent neutron experiments where softening of shear lattice vibrations in ice was enhanced with increasing pressure.<sup>8,9</sup> However, it is also interesting to consider mechanisms of pressure-induced amorphization in other water-based structures; recently, pressure-induced amorphization in tetrahydrofuran (THF) clathrate hydrates has been studied by x-ray and Raman techniques<sup>10</sup> and dielectric spectroscopy.<sup>11</sup> In many respects, clathrate hydrates' properties are very similar to ice. Indeed, it was first postulated in 1984 that THF hydrates would amorphize under pressure,<sup>2</sup> as has been observed.<sup>10,11</sup> Very recent experiments by Tulk *et al.*,<sup>12</sup> however, have shown that the frameworks in methane hydrates collapse under pressure; it was not possible to quench-recover the amorphized structure and, without exception, the original crystalline structures were recovered upon decompression. This suggests strongly that pressure amorphization does not constitute thermodynamic melting. A similar observation has been made for the silica analog of clathrate hydrate, clathrasils.<sup>13</sup> With the advance of high-pressure diffraction techniques, it has become possible recently to record diffraction patterns of pressure-collapsed structures. Significantly, *in situ* warming of the experimentally observed high-density amorphous methane hydrate phase by Tulk *et al.*<sup>12</sup> under pressure led to densification, exactly parallel to those in amorphous ices.<sup>2,3</sup> This novel phenomenon

provides an opportunity to compare the mechanisms for transformations between amorphous and crystalline forms of hydrate, ice, and silica analogs.<sup>10-14</sup> To this end, constant-pressure molecular dynamics (MD)<sup>15</sup> was used to explore phase space for pressure-induced amorphization and thermal annealing of methane hydrate. It will be shown that the local structures of water in the collapsed structures are different from amorphous ices. However, a very similar sequence of transformation was observed. Moreover, it is shown that amorphous clathrates can be converted back to the original crystalline form after removal of pressure. The results point unambiguously to neither the amorphization process nor amorphous structures having relevance to quenched liquid water-methane mixtures.

Classical constant-pressure MD was performed on a system of methane hydrate.<sup>15,16</sup> Details and the justification on the choice of the computational parameters are given in the Supplemental Material.<sup>17</sup> The water interaction was described by the TIP4P model,<sup>18</sup> with the OPLS-AA potential for methane-methane interactions<sup>19</sup> and water-methane potential parameters of Sun and Duan.<sup>20</sup> The simulation box was constructed from  $5 \times 5 \times 5$  replication of type-I unit cells. A large simulation box is necessary to avoid periodic size artifacts upon pressure compaction to an amorphous structure. The oxygen atoms' starting coordinates in the unit cell were taken from x-ray diffraction data.<sup>21</sup> The Rahman-Stillinger procedure was used to generate hydrogen atom positions with a negligibly small total dipole moment.<sup>22</sup> 90%-occupied systems ( $\text{CH}_4 \cdot 6.38\text{H}_2\text{O}$ ), prepared by random removal of methane from a fully occupied system, were studied; the typical composition of experimental hydrate samples is 85–95%. MD was performed at 3, 3.5, 4, 4.5, and 5 GPa at 80 K for up to 20 ns, or until amorphization occurred (if earlier than this). Post-amorphization annealing was achieved using the stabilized, amorphized structure at 3 GPa and heating in 20 K steps from 80 to 260 K at 5, 5.5, and 6 GPa for 0.2 ns at each step and then for up to a further 10 ns at 260 K (or until densification occurred). It was found that amorphization at 80 K occurred within 10 ns at 4 GPa, and 17 ns at 3.5 GPa; the predictions are in good agreement with the observed value of 3 GPa for  $\text{CD}_4 \cdot 6.26\text{D}_2\text{O}$ .<sup>12</sup> Within

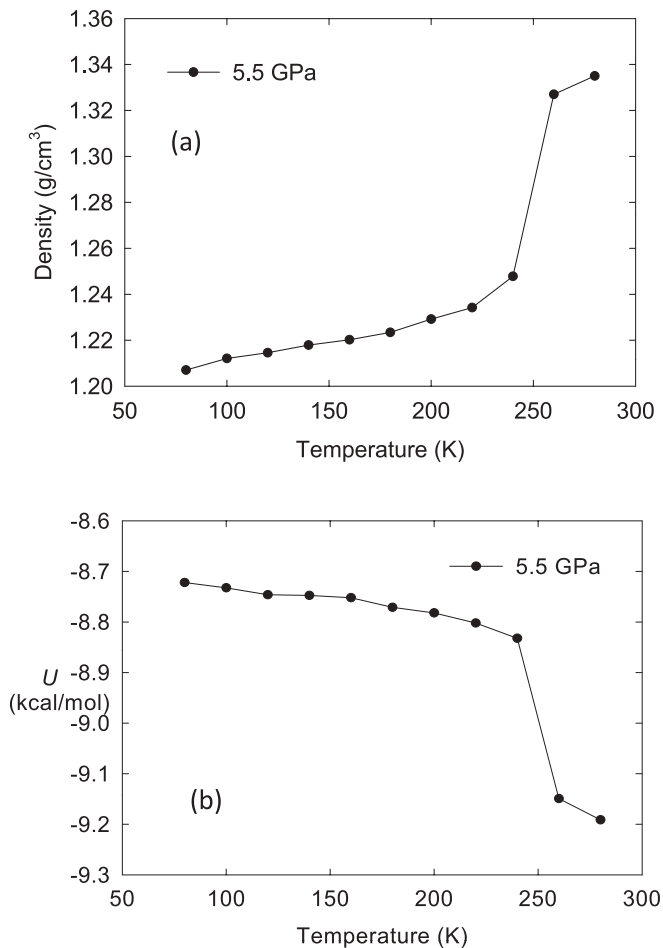


FIG. 1. (a) Density-temperature relationship for a series of simulations during the pressurized annealing process at 5.5 GPa towards the more dense amorphous hydrate form. (b) Potential energy (on a per-molecule basis, regardless of whether it is water or methane) as a function of temperature, during the high to very high density amorphous hydrate transition.

the 3.5–4.0 GPa range, the amorphized structures’ density is 1.20–1.22  $\text{g cm}^{-3}$ . This amorphous form’s annealing at 5.5 and 6 GPa exhibited densification to 1.32–1.34  $\text{g cm}^{-3}$  within around 7 and 4 ns, respectively, at 260 K, with none evident at 5 GPa (within 10 ns), in essential agreement with experimental densification at 250 K and 5 GPa,<sup>12</sup> and similar to HDA  $\rightarrow$  VHDA transition.<sup>23</sup> To investigate densification transition’s nature, longer simulations of up to 10 ns were performed from 80 to 280 K at 5.5 GPa, and the resultant relaxed densities are shown in Fig. 1(a), characteristic of a first-order-like phase transition. The calculated configurational energies along the annealing path [see Fig. 1(b)] show the higher-density form is more energetically stable, despite more strained hydrogen bonding and a slightly greater number of nearest-neighboring water molecules.

Comparisons of the water-water pair distribution functions (PDFs) are shown in Fig. 2 for  $g_{\text{OO}}(r)$ ,  $g_{\text{OH}}(r)$ , and  $g_{\text{HH}}(r)$  between ambient-pressure crystalline (sI) hydrate at 80 K with the amorphous form at that temperature (and 3 GPa) and the more dense form at 260 K (and 5.5 GPa) with those of water-methane,  $g_{\text{OC}}(r)$  and  $g_{\text{CH(w)}}(r)$ , and of the methane-methane

distribution  $g_{\text{CC}}(r)$ ; water-water distributions are shown on the left, while methane-water and methane-methane data are on the right. From  $g_{\text{OO}}(r)$ , it is clear that the crystalline lattice of the hydrate framework has been destroyed, while nonzero  $g_{\text{OH}}(r)$  beyond the first coordination shell (for 2.2–2.4 Å) points towards more strained hydrogen bonding and more than four water molecules are in the nearest-neighbor environment. For the amorphous structures, the water-water PDFs are essentially featureless beyond around 4–4.5 Å. Although this is in qualitative agreement with experimental data for structure and PDFs of amorphous ices as found by Bowron *et al.*,<sup>24</sup> there are clear differences within the first 4 Å. It is worth noting that there is a somewhat larger value for  $g_{\text{OO}}(r)$  for the more dense amorphous form at 3 Å not observed in the lower-density amorphous hydrate, together with a reduced  $g_{\text{OH}}(r)$  at this separation [see Figs. 2(a) and 2(b)]: This is due to more strained hydrogen bonding in the more dense amorphous case and more than four nearest-neighboring water molecules. The integrated O-O coordination number out to 3.3 Å is 5.76 (at 3.3 GPa and 80 K) and 6.02 (at 5.5 GPa and 260 K) for the high and very high density phases, respectively. The corresponding coordination numbers in recovered HDA and VHDA ice are 5.0 and 5.8.<sup>25,26</sup> Obviously, the more open hydrate cage structure permits more water molecules to be compressed into the immediate environment. The difference of O-O coordination between the high and very high density amorphous hydrate forms is, however, substantially smaller than in amorphous ices. This indicates that the local water structures of water in ice and hydrate are quite different. Indeed, it is difficult to reconcile that if amorphized hydrate were simply a melted mixture of methane and water, then the structure of the “water” could be so different from that of the amorphous ices.<sup>25,26</sup>

From the water-methane and methane-methane PDFs [Figs. 2(e) to 2(g)], it is seen readily that the cages have collapsed, the guest and water are in intimate contact, and the distance between methanes is reduced substantially resulting in a dense amorphous structure. It is noteworthy that the closest water-methane contacts in both cages are about 3.20 Å and are shorter than the sum of the respective van der Waals radii ( $\text{CH}_4$ , 2.0 Å; O atom, 1.59 Å). The short separation indicates the methane-water interaction is repulsive. Significantly, unlike a liquid, the disordering is not totally random. The heights of the PDF peaks before and after amorphization are very similar, indicating that the methane molecules are still at the centers of collapsed cages, and that the C-C distribution itself is largely unaffected, although shifted to lower separations commensurate with densification of the collapsed, amorphous lattice. This point is exemplified by consideration of the static structure factors,  $S_{\text{C}}(\mathbf{k})$ , from the carbon-atom density-correlation function<sup>15</sup> [Fig. 3(a)]. The structure factor is simply shifted to slightly larger values of momentum transfer,  $\mathbf{k}$ , consistent with densification, but  $S_{\text{C}}(\mathbf{k})$  itself remains similar, albeit with fewer distinct features above 4 Å<sup>-1</sup>, due to less regular placement of carbon atoms on a “crystallographic grid” of cage centers in sI. It was also found from methane velocity correlation functions (not shown) that guest rotational motion was hindered substantially with rotational motion times 2.5–3 times slower than almost-free rotation in sI.

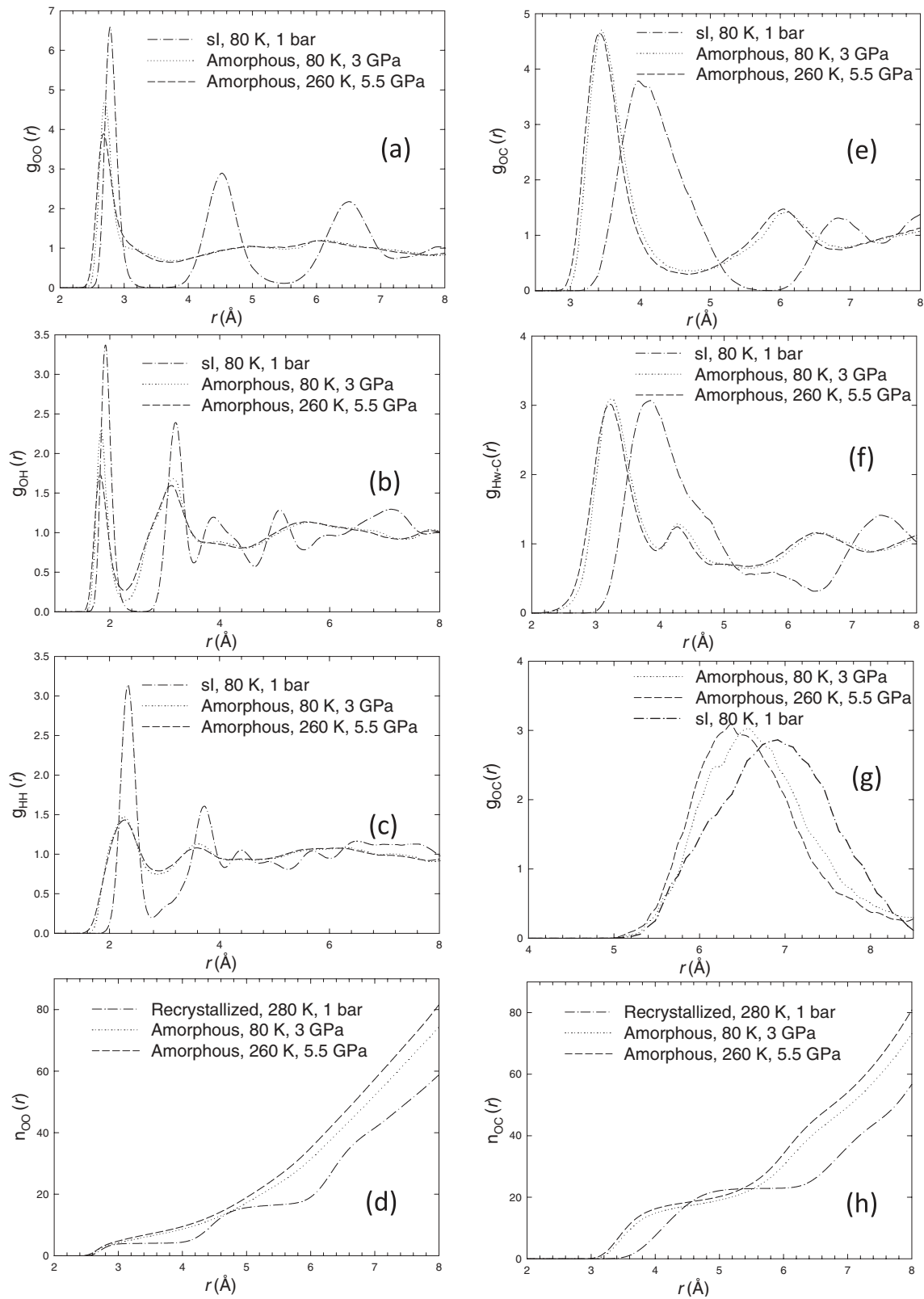


FIG. 2. (a) Water-water O-O PDFs for ambient-pressure crystalline (sl) hydrate at 80 K, along with the amorphous form at that temperature (and 3.5 GPa) and the more dense amorphous form at 260 K (and 5.5 GPa). (b) Water-water O-H PDFs. (c) Water-water H-H PDFs. (d) Coordination numbers for O-O for the amorphous form at 80 K and 3.5 GPa and the more dense amorphous form at 260 K and 5.5 GPa, along with the recrystallized form. (e) Water-methane O-C PDFs. (f) Water-methane H<sub>W</sub>-C PDFs. (g) Methane-methane C-C PDFs. (h) Coordination numbers for O-C for the amorphous form at 80 K and 3.5 GPa and the more dense amorphous form at 260 K and 5.5 GPa, along with the recrystallized form.

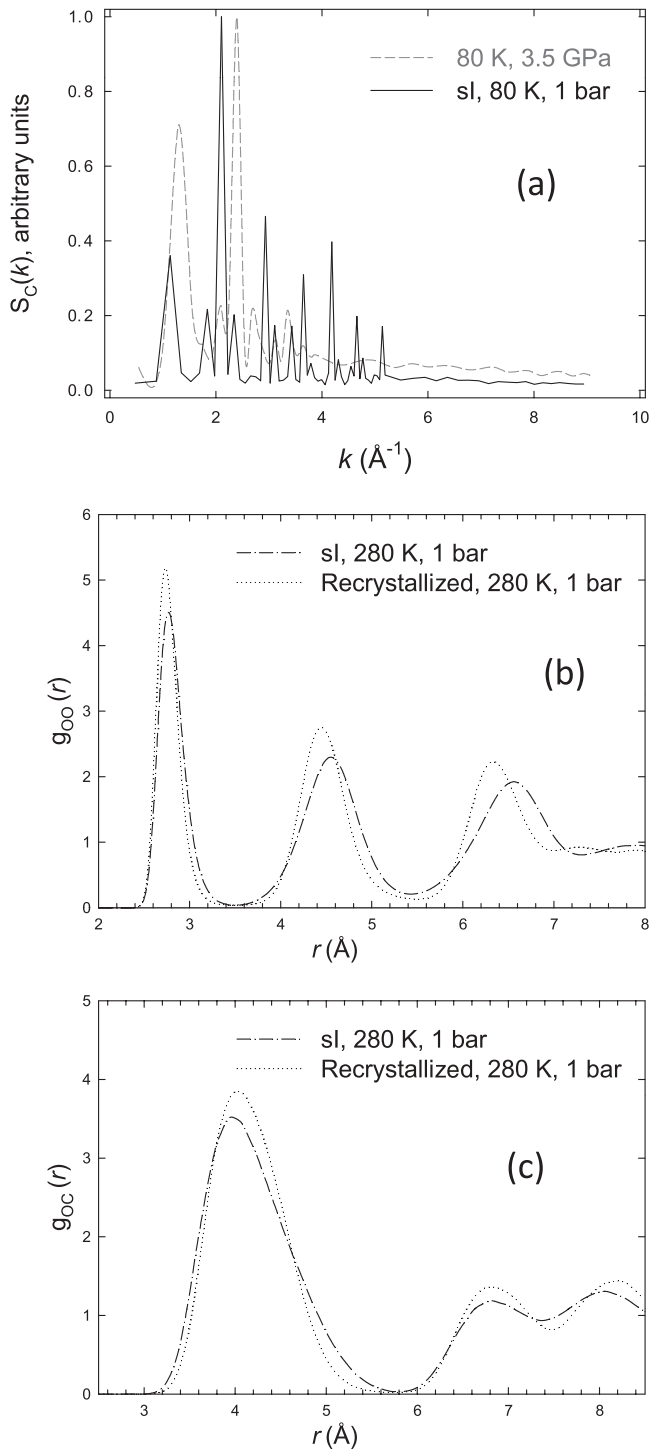


FIG. 3. (a) Carbon-atom static structure factor for the ambient-pressure sI system and the amorphous, 3.5 GPa system at 80 K. (b) Water-water O-O PDFs for ambient-pressure crystalline (sI) hydrate at 280 K, along with the recrystallized form from the more-dense amorphous state (260 K, 5.5 GPa) at the same conditions (280 K, 1 bar). (c) Water-methane O-C PDFs for the recrystallized system.

To characterize the short-range environment in the 2.4–3.8  $\text{\AA}$  range, O-O spatial distribution functions (SDFs)<sup>27</sup> are compared in Fig. 4 at different O-O distances for high and very high density amorphous hydrates (80 K at 3.5 GPa and

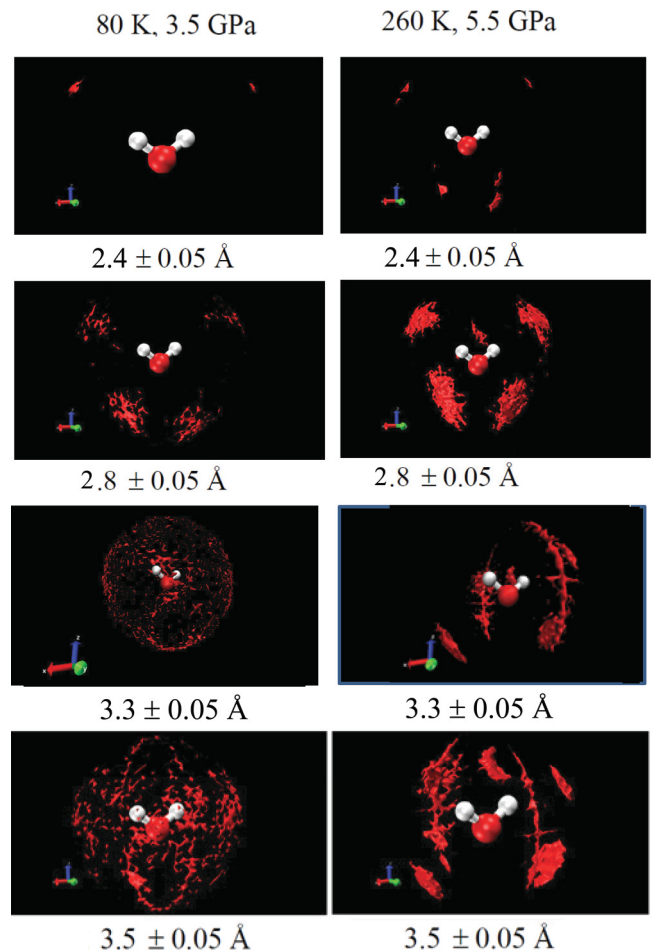


FIG. 4. (Color online) Spatial distribution function (SDF) at various O-O separations ( $\pm 0.05 \text{\AA}$ , i.e., a spherical shell width of  $0.1 \text{\AA}$ ) for high and very high density amorphous hydrate in the local frame of the water molecule (left and right panels, respectively). The contour surfaces represent SDF values above a threshold such that 30% of the molecules are represented.

260 K at 5.5 GPa, respectively). For a given O-O separation, it is clear that the probability of a nearby water’s oxygen being present is substantially larger in the very high density form vis-à-vis the high-density case. At an O-O distance of  $2.80 \pm 0.05 \text{\AA}$  (i.e., 2.75–2.85  $\text{\AA}$ ), in addition to the four “lobes” indicative of the near-tetrahedral environment, the “foray” of a fifth water into the nearest-neighbor shell<sup>24</sup> is already evident in the very high density structure. At longer O-O separations of 3.3 and  $3.5 \pm 0.05 \text{\AA}$ , more waters are “forced” into the coordination shell, but the SDFs for the two amorphous forms differ significantly. The seemingly uniform SDF surrounding the oxygen in the high-density form suggests the longer-range distribution is disordered. In contrast, the more spatially localized features in SDF of the very high density form reflect a high degree of local ordering. The SDFs exhibit thermal annealing of the high-density amorphous form at high pressure, resulting in relaxation to a more ordered structure, consistent with observations of lower configurational energy [Fig. 1(b)].

To assess the dense hydrates’ stability, both amorphous structures were relaxed at 280 K and 1 bar pressure (under the

potential model's melting point). Within several nanoseconds, both structures relaxed to one relatively close to sI, with a density of 0.96 g/cm<sup>3</sup>, compared to 0.91 g/cm<sup>3</sup> for sI. Typical PDFs are presented in Figs. 3(b) and 3(c) for the sI structure along with that recovered from the 1.32 g cm<sup>-3</sup> density amorphous structure (at 260 K and 5.5 GPa), with further data in Figs. S1 and S2 (Supplemental Material).<sup>17</sup> The strong resemblance suggests a largely restored sI structure with local cage distortions in an imperfect host lattice and some still partially collapsed cages; the lack of large differences in the O-C PDF of Fig. 3(c) reveals that no water molecules have remained in close contact with the methane molecules or "inside" reformed cages. This finding mirrors reversible crystallization found in all clathrate hydrates<sup>9</sup> and analogous amorphized silica clathrasils;<sup>13</sup> however, empty (guest-free) clathrasils were found to undergo irreversible amorphization; i.e., guests inside the cavities were found to constitute "organizing centers" for reversible transformation. It is appropriate to compare this further to amorphization of ices and THF hydrates. This transition from ice-Ih is irreversible upon decompression,<sup>2,3,14,28</sup> while pressure-amorphized THF hydrate was irreversible if recovered at 1 bar and at 25 K<sup>10</sup> but reversible when warm to 110 K.<sup>10,11</sup> This reinforces the observation<sup>13</sup> on cavity-occupied clathrasils that guests allow for reversible transformation, as observed in these results for methane hydrate and by experiment. It is difficult to compare the structural features of amorphous methane hydrates studied in this work with experimental data for THF hydrate due to the resolution of x-ray data,<sup>10,11</sup> although there is good agreement between the observed general structural features gleaned from the amorphous methane hydrate forms' PDFs and SDFs from the simulations of this study and general findings from neutron diffraction results and experimental structure factors.<sup>12</sup> Larger O-O coordination numbers for amorphous hydrates vis-à-vis

HDA and VHDA ices reflects the nature of the more open hydrate cage structure allowing more water molecules to be compressed into the immediate environment, which is reflected in SDFs of the higher-density amorphous hydrate (Fig. 3), with more prominent evidence of the fifth water molecule as compared to experimental SDFs of HDA and VHDA ices.<sup>25,26</sup>

The recent experimental findings<sup>12</sup> on amorphization and subsequent transformation to a very high density hydrate form have been reproduced, almost quantitatively. Although the transformation sequence of methane hydrate is identical to ice, the water structures of the densified amorphous hydrates are different from the corresponding HDA and VHDA ices.<sup>24-26</sup> Significantly, long-range correlation between the methane positions is maintained. Amorphized hydrates cannot be assumed to be arrested disordered liquid mixtures. In view of the almost parallel behavior of ice and hydrate under pressure and annealing, the present results suggest strongly that pressure-induced amorphization of ice is a nonequilibrium process and that the various amorphous phases are merely kinetic products. Amorphous clathrates revert back to their crystalline structure at 80 K when the pressure is lifted.<sup>12</sup> The results reinforce the mechanical instability mechanism<sup>7,8,26</sup> and lend support to viewing pressure amorphization of crystalline ice to HDA and subsequent recovery of LDA via decompression to zero pressure as kinetically controlled processes; however, it should be pointed out that some care should be taken in this conclusion, in that simulation at one temperature does not exclude the possibility of thermal melting at higher temperature. Nonetheless, the evidence of this study suggests that LDA ice may simply be incompletely relaxed ice Ih. The observed hysteresis is akin to van der Waals looping.<sup>6</sup> This interpretation would cast doubt on the "two-liquid" water hypothesis's fundamental assumptions.<sup>4</sup>

\*niall.english@ucd.ie

†john.tse@usask.ca

<sup>1</sup>P. H. Poole, F. Sciortino, U. Essmann, and H. E. Stanley, *Nature (London)* **360**, 324 (1992).

<sup>2</sup>O. Mishima, L. D. Calvert, and E. Whalley, *Nature (London)* **310**, 393 (1984).

<sup>3</sup>O. Mishima, L. D. Calvert, and E. Whalley, *Nature (London)* **314**, 76 (1985).

<sup>4</sup>O. Mishima and H. E. Stanley, *Nature (London)* **396**, 329 (1998).

<sup>5</sup>J. S. Tse, *J. Chem. Phys.* **96**, 5482 (1992).

<sup>6</sup>J. S. Tse, D. D. Klug, M. Guthrie, C. A. Tulk, C. J. Benmore, and J. Urquidi, *Phys. Rev. B* **71**, 214107 (2005).

<sup>7</sup>T. Strässle, A. M. Saitta, S. Klotz, and M. Braden, *Phys. Rev. Lett.* **93**, 225901 (2004).

<sup>8</sup>T. Strässle, S. Klotz, G. Hamel, M. M. Koza, and H. Schober, *Phys. Rev. Lett.* **99**, 175501 (2007).

<sup>9</sup>Y. P. Handa, J. S. Tse, D. D. Klug, and E. Whalley, *J. Chem. Phys.* **94**, 623 (1991).

<sup>10</sup>Y. Suzuki, *Phys. Rev. B* **70**, 172108 (2004).

<sup>11</sup>O. Andersson and G. P. Johari, *J. Chem. Phys.* **129**, 234505 (2008).

<sup>12</sup>C. A. Tulk, D. D. Klug, J. J. Molaison, A. M. dos Santos, and N. Pradhan, *Phys. Rev. B* **86**, 054110 (2012).

<sup>13</sup>J. S. Tse, D. D. Klug, J. A. Ripmeester, S. Desgreniers, and K. Lagarec, *Nature (London)* **369**, 724 (1994).

<sup>14</sup>T. Loerting, C. G. Salzmann, K. Winkel, and E. Mayer, *Phys. Chem. Chem. Phys.* **8**, 2810 (2006).

<sup>15</sup>D. Frenkel and B. Smit, *Understanding Molecular Simulations* (Academic Press, New York, 2002).

<sup>16</sup>J. S. Tse and M. L. Klein, *Phys. Rev. Lett.* **58**, 1672 (1987).

<sup>17</sup>See Supplemental Material at <http://link.aps.org/supplemental/10.1103/PhysRevB.86.104109> for additional details on methodology and additional figures comparing the structure of recrystallized methane hydrate with the starting crystal structure.

<sup>18</sup>W. L. Jorgensen *et al.*, *J. Chem. Phys.* **79**, 926 (1983).

<sup>19</sup>W. L. Jorgensen, D. S. Maxwell, and J. Tirado-Rives, *J. Am. Chem. Soc.* **118**, 11225 (1996).

<sup>20</sup>R. Sun and Z. H. Duan, *Geo. Cos. Acta* **69**, 4411 (2005).

<sup>21</sup>R. K. McMullan and G. A. Jeffrey, *J. Chem. Phys.* **42**, 2725 (1965).

<sup>22</sup>A. Rahman and F. H. Stillinger, *J. Chem. Phys.* **57**, 4009 (1972).

<sup>23</sup>T. Loerting, C. Salzmann, I. Kohl, E. Mayer, and A. Hallbrucker, *Phys. Chem. Chem. Phys.* **3**, 5355 (2001).

<sup>24</sup>D. T. Bowron *et al.*, *J. Chem. Phys.* **125**, 194502 (2006).

- <sup>25</sup>J. L. Finney, A. Hallbrucker, I. Kohl, A. K. Soper, and D. T. Bowron, *Phys. Rev. Lett.* **88**, 225503 (2002).
- <sup>26</sup>J. L. Finney, D. T. Bowron, A. K. Soper, T. Loerting, E. Mayer, and A. Hallbrucker, *Phys. Rev. Lett.* **89**, 205503 (2002).
- <sup>27</sup>I. M. Svishchev and P. G. Kusalik, *J. Chem. Phys.* **99**, 3049 (1993).
- <sup>28</sup>T. Loerting, K. Winkel, M. Seidl, M. Bauer, C. Mitterdorf, P. H. Handlr, C. G. Salzmann, E. Mayer, J. L. Finney, and D. T. Bowron, *Phys. Chem. Chem. Phys.* **13**, 8783 (2011).